JOURNAL OF AIRCRAFT
Vol. 45, No. 6, November–December 2008

Oscillation Effects on Boundary-Layer Development Under the Influence of Favorable Pressure Gradients

M. Amir*
University of Southampton, Southampton, England SO17 1BJ United Kingdom
and
K. Kontis†
University of Manchester, Manchester, England M60 1QD United Kingdom

DOI: 10.2514/1.35532

An experimental study has been conducted to investigate the effects of oscillation at a range of Strouhal numbers (0.0006 to 0.0113) on the boundary-layer development of a flat plate under the influence of favorable pressure gradients. The Reynolds number was 10^6 based on the flat-plate chord length. An inverted airfoil placed in the turbulent region over the flat plate was used to create the effects of favorable pressure gradients. Hot-wire anemometry was used to measure the velocities in the streamwise direction. The flow separates near the rounded leading edge, causing the formation of the separation bubble. It is found that the time-averaged velocity and turbulence intensity profiles remain mostly unaffected by oscillation in the turbulent flow regions (II and III). The boundary-layer properties such as the boundary-layer displacement thickness, momentum thickness, and the shape factor remain almost constant. However, in region I, in which the flow is in its transitional state, oscillation slows the reattachment process under the influence of favorable pressure gradients.

Nomenclature

A	=	amplitude of oscillation
F	=	frequency of oscillation
H	=	shape factor
ℓ	=	length of the flat plate
P	=	local static pressure
P_∞	=	freestream static pressure
Re_N	=	Reynolds number
S_t	=	Strouhal number, (F^*A/U_∞)
t	=	time
U_{rms}	=	root-mean-square velocity
U_∞	=	freestream velocity
u	=	mean velocity
x	=	horizontal distance along the flat plate
x_{tran}	=	transition point
y	=	vertical distance above the flat plate
$\Delta\delta$	=	increase in boundary-layer thickness
δ	=	boundary-layer thickness
δ^*	=	displacement thickness
θ	=	momentum thickness
ν	=	kinematic viscosity of air
ω	=	angular velocity

I. Introduction

EVER since the introduction of the boundary-layer concept, there has been a constant challenge faced by scientists and engineers to minimize its adverse effects and control it to their advantage. A main objective of a control procedure is to prevent or at least delay the separation of the boundary layer from the wall. Methods employing suction, blowing, vortex generators, turbulence promoters, etc., have been investigated and applied extensively with a varying degree of success. However, the use of a moving or oscillating wall for boundary-layer control has received relatively little attention, and there are many unanswered questions associated with the effects of oscillation on the boundary-layer development, especially under the presence of adverse pressure gradients. A moving surface attempts to accomplish this in two ways:

1) It retards the growth of the boundary layer by minimizing the relative motion between the surface and the freestream.

2) It adds momentum into the existing boundary layer.

Boundary-layer control by a moving surface was first demonstrated by Favre [1]. Favre ran an endless belt forming a portion of the upper surface of an airfoil and delayed separation until high angles of attack. Since that initial study, boundary-layer control by surface motion has been examined and successfully demonstrated in a number of similar applications [2,3]. In those studies, however, the moving-wall effects on the boundary layer itself have not been thoroughly examined.

For flows over moving walls, the point or line of vanishing wall shear does not necessarily coincide with separation, and this greatly complicates the problem. This was first observed by Rott [4] while analyzing the unsteady flow in the vicinity of a stagnation point. He observed that although the wall shear vanished with an accompanying reverse flow, there was no singularity or breakdown of the boundary-layer assumptions. Seeking a generalized model for separation, Sears [5] postulated that the unsteady separation point is characterized by the simultaneous vanishing of the shear and the velocity at a point within the boundary layer as seen by an observer moving with the velocity of the separation point. While investigating a steady flow over a moving wall, Moore [6] arrived at the same model for unsteady separation. On the basis of an intuitive relationship between steady flow over a moving wall and unsteady flow over a fixed wall, Moore was able to sketch the expected velocity profiles for both cases. He considered the possibility that a Goldstein-type singularity occurred at the location in which the velocity profile simultaneously had zero velocity and a shear at a point above the moving wall. Equivalently, for unsteady separation on a fixed wall, the separation point was the location at which both the shear and velocity vanished in a singular fashion in a frame of reference moving with the separation point. The main drawback of this Moore–Rott–Sears model in the fixed-wall case was that the speed of the separation of point was known a priori, making it difficult to locate this point and forcing researchers to rely on more qualitative measures for unsteady separation.

Received 6 November 2007; accepted for publication 27 June 2008.

*Research Fellow, School of Engineering Sciences; m.amir@soton.ac.uk.
†Reader, Head of Aerospace Research Group and Aero-Physics Laboratory, School of Mechanical, Aerospace and Civil Engineering; k.kontis@manchester.ac.uk. Senior Member AIAA.

Moving walls have recently been employed by Bott and Bradshaw [7] to study the effect of high freestream turbulence on boundary layers as well as by Uzkan and Reynolds [8], Thomas and Hancock [9], and Aronson et al. [10] to study the interaction of turbulence with a wall. In these studies, however, the incident boundary layer was removed and no upstream induced velocity defect existed over the moving wall. When the wall speed equaled the freestream speed, a shear-free boundary layer developed on the moving wall. Because of their importance as a means of improving near-wall turbulence models, such shear-free boundary layers have been studied theoretically by Hunt and Graham [11] as well as computationally by Perot and Moin [12].

A recent appraisal of the effects of wall oscillation on turbulent flows has been published by Karniadakis and Choi [13], in which connection is made with drag-reduction techniques, such as the excitation of the near-wall flow by transverse traveling waves [14]. Choi et al. [15] measured the streamwise variation of wall-shear stress over an oscillating plate in the turbulent boundary layer, showing that the skin-friction coefficient is reduced by as much as 45% over the oscillating wall as compared with that over the stationary wall. Choi and Clayton [16] proposed a mechanism of turbulent drag reduction based on the hot-wire anemometry and the flow-visualization study of the near-wall turbulence structure over the oscillating wall, suggesting that a negative spanwise vorticity that is generated at the edge of the viscous sublayer plays a significant role in reducing the skin-friction drag of the turbulent boundary layer.

Spanwise oscillations therefore have successfully demonstrated the reduction of skin-friction drag, but no such attempts have been made with streamwise oscillations. Also, a very limited amount of published work exists in the literature regarding models undergoing oscillations in the streamwise direction. Very recently, in our previous studies [17], we noticed that streamwise oscillation under the influence of adverse pressure gradients caused increased levels of pressure on the entire length of the flat plate. The pressure peak increased in magnitude due to oscillation. At different points during the oscillation cycle, the peak also varied in magnitude. Behind the cylinder, there was a continuous rise in pressures up to the trailing edge of the plate. With increasing amplitude, a displacement of the pressure peak from its mean position occurred. The strongest effect took place at Strouhal number $S_t = 0.0038$. Just ahead of the cylinder, the boundary-layer thickness increased due to oscillation. However, with increasing S_t, the effects were getting smaller. Downstream of the cylinder, the boundary layer remained unaffected by oscillation. At higher amplitudes, the boundary-layer thickness increased near the leading edge. Also, at higher amplitudes, the flow in the leading-edge region exhibited an oscillatory behavior, with the number of cycles increasing with increasing Strouhal number. This was associated with the presence of the separation bubble and the influence that the flat-plate oscillation may have on its structure, properties, and characteristics.

The purpose of the present study is therefore, to examine the effects of flat-plate oscillation on the boundary-layer development under the influence of favorable pressure gradients.

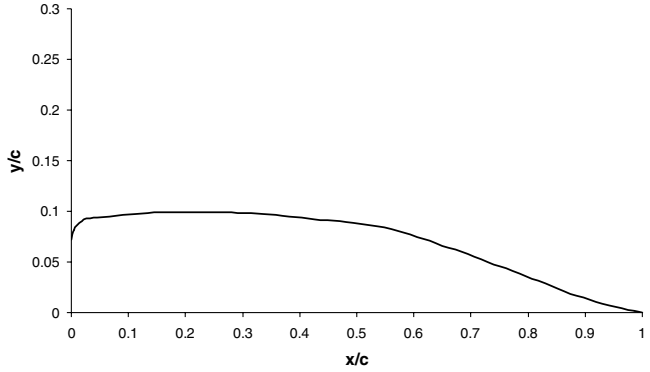

Fig. 1 Chordwise profile of the inverted airfoil.

II. Experimental Setup and Apparatus

The experiments were conducted in a low-speed subsonic wind tunnel. The tunnel has a test section of 1.4 (length) by 0.45 (width) by 0.45 m (height). The ceiling and side walls are made of high-transparency Perspex to allow optical access. The contraction ratio of the nozzle is 6.5 to 1, and the maximum velocity of the test section is 32 m/s. The freestream turbulent intensity of the tunnel (in the absence of the model) is less than 0.15%. All measurements were taken at a freestream velocity of 16 m/s. The experiments were performed at a Reynolds number equal to 10^6 based on the plate chord length. A 1-m-long flat plate made of aluminum was used, with its width covering the entire test section, placed 0.16 m above the floor of the test section. Its surface had a smooth finish. It was placed on linear bearing rods to minimize friction and ensure its oscillation in the x (streamwise) direction. The oscillation mechanism was installed underneath the wind-tunnel working section with the flat-plate model attached on the top. The whole system rested on a heavy metal base plate to avoid unwanted vibrations at higher frequencies of operation. The flat-plate model was made to oscillate at a range of frequencies of 0 to 6 Hz and amplitudes of 0 to 0.03 m. Table 1 summarizes the cases tested with oscillation.

To produce the effects of favorable pressure gradients, a half-airfoil section was placed under the top section of the wind tunnel. The airfoil was placed in an inverted position in different regions of the flow. Figure 1 shows the profile of the airfoil section.

In our previous investigation [17], we found that from both oil-flow visualization and hot-wire anemometry that the boundary in region I was transitional. In region III, the boundary layer was turbulent (fully developed), whereas in region II, the boundary layer was still at the late stages of its transition to turbulence (Fig. 2). The physical implications of the three flow regions were discussed in [17].

To measure the surface pressure on the flat plate, pressure taps were drilled along its midchord. The taps were therefore placed along the centerline of the plate at a distance of 20 mm from each other in

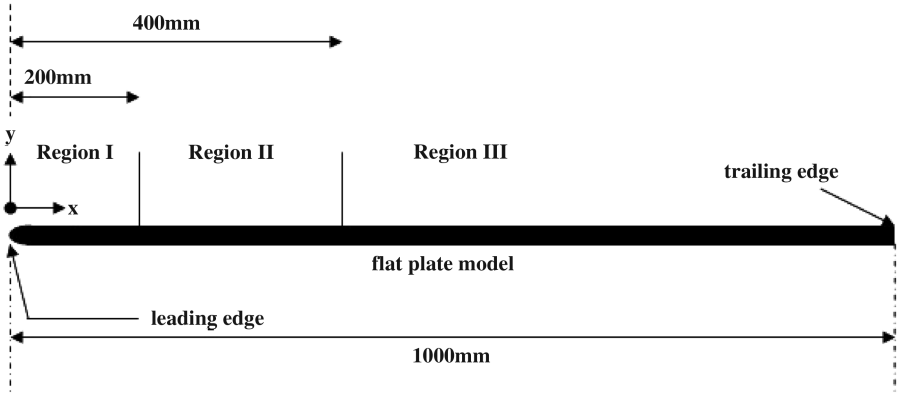

Fig. 2 Different flow regions over the flat plate.

the turbulent region. Near the leading edge and in the transition region, pressure taps were placed at shorter distances from each other. In total, 65 pressure tappings were used. The diameter of each tapping was 1 mm and the length was approximately 15 mm. The tapping location is shown in Fig. 3. Pressure transducers were used to measure the pressure distribution and were connected to the tappings via plastic tubes.

To measure the boundary-layer profiles, a single-probe hot-wire system was used. The hot-wire probe was mounted from the top of the wind tunnel. A horizontal slot that ran along the length of the test section was created on the top window. The probe was passed through the slot and into the test section. Attached to the probe was a traverse device that moved the probe to the desired location along the flat plate. A microgauge was connected to this system to monitor the vertical distance of the hot wire from the flat plate during the measurements. A PC with a data acquisition system was set up to capture the data. The data from the pressure transducers and the hot-wire probe were captured using LabVIEW 7.1 software.

To record the mean pressure, a sampling rate of 2 kHz was used over of a period of 2 s. The estimated overall accuracy for the pressure measurements was $\pm 3.5\%$. A static calibration of the hot wire, based on King's law, was obtained by placing the probe in the freestream at the start of the working section. The instrument uncertainty in the velocity measurements was found to be $\pm 2.5\%$. A sampling rate of 2 kHz over a period of 2 s was used to record the mean velocities from the hot-wire system.

To force transition, the flat-plate model used in this research had a rounded nose at the front. The flow separated very near the rounded leading edge, causing the formation of the separation bubble. The length of the leading-edge separation bubble was then measured. The oil-flow picture in Fig. 4 shows a close-up view of the leading-edge separation bubble. The maximum length of the separation bubble was observed at the center (midchord) of the flat plate. It was found to be 18.5 mm in length. It is also evident from Fig. 4 that the separation bubble does not start exactly at the leading edge but at some distance away from it; this was measured to be around 10 mm from the leading edge.

III. Measurement Techniques and Error Analysis

In addition to the pressure transducers, a liquid manometer rake was also employed (mainly for stationary measurements) to obtain the pressures on the flat plate. The liquid manometer rake had only 36 manometers, whereas the flat plate had a total of 65 pressure tappings

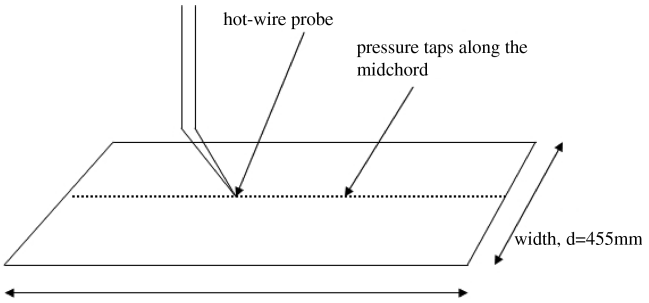

Fig. 3 Schematic of the experimental layout showing location of pressure tappings.

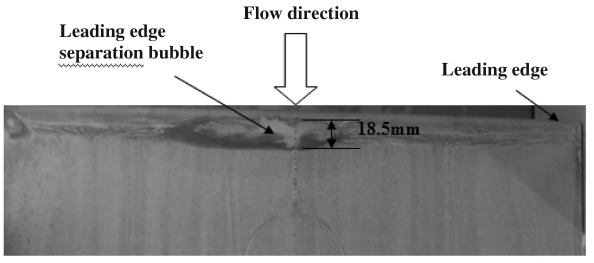

Fig. 4 Close up view of the leading-edge separation bubble.

along its centerline. The measurements were therefore taken in two halves for each condition. Similarly, a total of 5 pressure transducers were used a number of times to obtain a complete set of pressure data for each condition. By employing this method, the accuracy of the results is slightly reduced. In both measurement techniques, the pressure was measured relative to atmosphere.

To calculate C_p, a reference pressure (freestream static pressure P_∞ in this case) was measured by placing a pitot-static tube ahead of the leading edge of the flat plate inside the test section. It is usually more difficult to accurately measure the freestream static pressure.

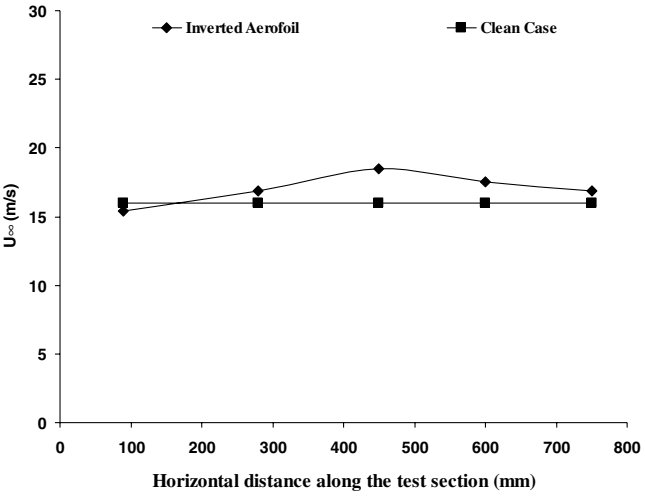

Fig. 5 Effects of the inverted airfoil on the freestream velocity along the test section.

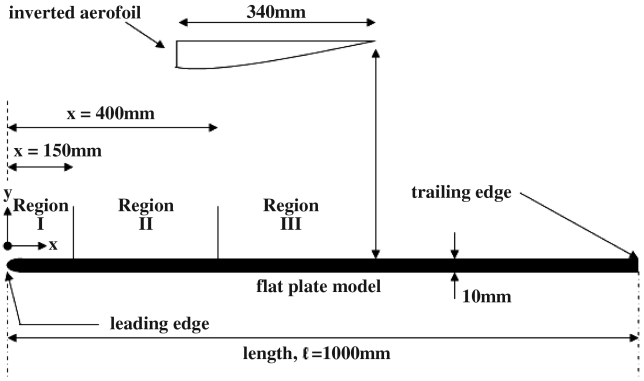

Fig. 6 Locations of the inverted airfoil and the three flow regions.

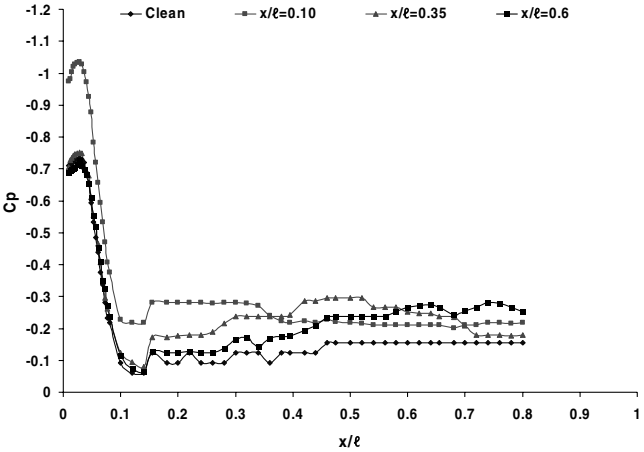

Fig. 7 Effects of the inverted airfoil on surface pressure along the flat plate.

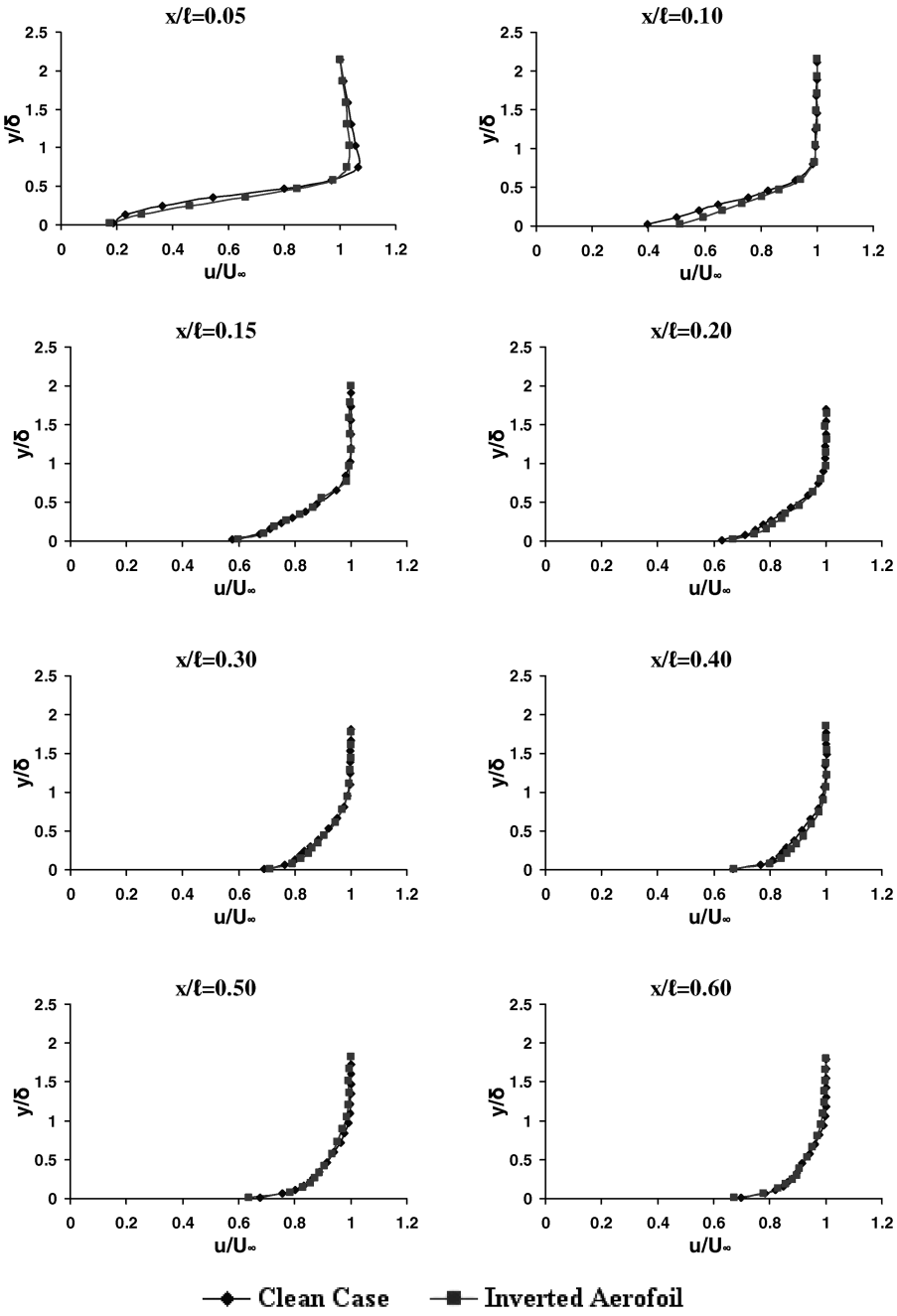

Fig. 8 Effects of the inverted airfoil on the mean velocity profiles.

The difference between the true P_∞ and the measured P_∞ may be due to one or all of the following: 1) misalignment of the tube axis and the flow-velocity vector, 2) finite tube diameter,[‡] and 3) influence of the tube-support leading edge.

A conventional single-probe hot wire was used for velocity measurements. It is important to note that a conventional hot-wire probe cannot distinguish the direction of the flow, due to the directional symmetry of the wire element. As a consequence, measurements with such a probe in separated flows, displaying regions with reverse flow, will give erroneous results. One such flow case that has been extensively studied both experimentally and numerically over the past decades is the laminar separation-bubble flow caused by an adverse pressure gradient. The insensitivity of the single hot wire to the direction of the flow (for example, in the laminar separation bubble) gives erroneous measurements of the mean and the rms of the streamwise velocity in the low-velocity region close to the wall on which reverse flow occurs. In transition experiments in which the evolution in the separation bubble of different types of artificially generated deterministic disturbances is studied, the directional insensitivity will lead to an uncertainty of the behavior and structure of these disturbances.

[‡]Streamlines next to the tube must be different from those in the undisturbed flow; hence, the mere presence of the probe results in a static pressure value that is different from the actual pressure of the undisturbed flow.

IV. Results and Discussion

A. Case A: No Oscillation

1. Surface-Pressure Measurements

Surface pressure was measured along the midchord of the flat plate. In the practical wind-tunnel measurements on the flow around aerodynamic bodies, pressure distributions are generally presented in terms of pressure coefficient C_p. The pressure coefficient is defined by Eq. (1). $C_p = 1$ at a stagnation point and $C_p = 0$ at a far distance from the body, where the freestream velocity is undisturbed:

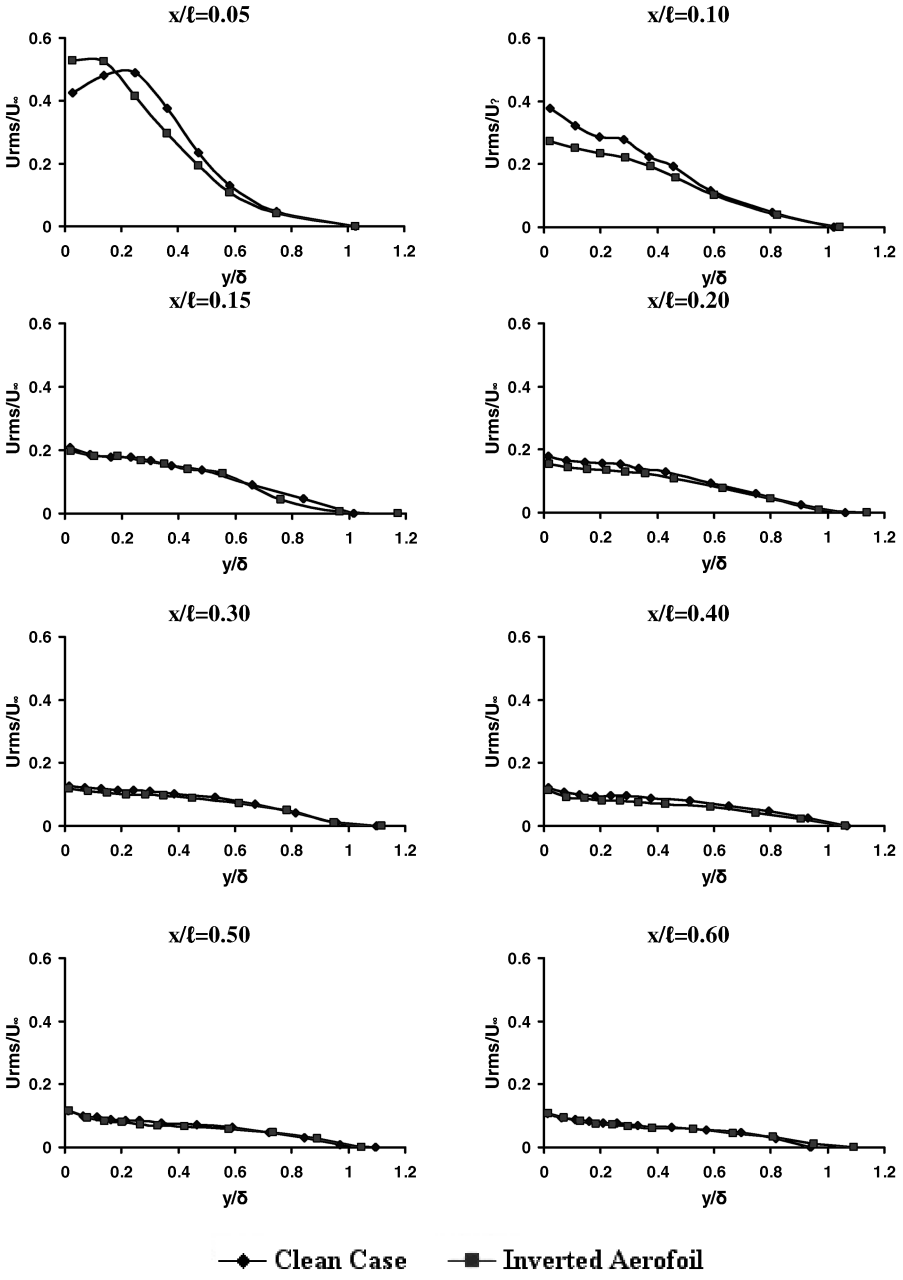

Fig. 9 Effects of the inverted airfoil on the turbulence intensity profiles.

$$C_p = \frac{P - P_\infty}{1/2\rho U_\infty^2} \tag{1}$$

where P is the local static pressure, P_∞ is the freestream static pressure, ρ is the freestream density, and U_∞ is the freestream velocity.

The present research involves a leading-edge separation bubble on the flat-plate model. Crompton and Barrett [18] carried out an investigation of the separation bubble formed behind the sharp leading edge of a flat plate at a number of incidence angles. Their results showed that the minimum pressure occurred over the front portion of the bubble, in which there is a pressure plateau. This was followed by a region of strong pressure recovery up to and beyond reattachment, with a zero pressure gradient further downstream. The maximum adverse pressure gradient existed just before the reattachment point, and the relaxation of the turbulent boundary layer occurred mainly in the zero pressure gradient. When the flat plate was placed at a 0 deg incidence angle, C_p was approximately -0.85 under the separation bubble and the pressure recovered back to a value of $C_p = -0.15$ close to the trailing edge.

One of the first tests that were performed with the inverted airfoil was to examine the effects it had on the freestream velocity inside the working section. A comparison was therefore made between the freestream velocities with and without the presence of the inverted airfoil. The inverted airfoil was kept in region II. Figure 5 shows the increased freestream velocities both upstream and downstream of the location of the inverted airfoil. The maximum effect is observed just underneath the middle section of the inverted airfoil. The local freestream velocity at this point is 18.5 m/s, compared with the freestream value of 16 m/s for the clean case.

The effects of the inverted airfoil were examined on the surface-pressure distribution along the flat plate. Figure 6 shows the locations of the airfoil relative to the three flow regions over the flat-plate model. It can be seen in Fig. 6 that when the leading edge of the airfoil is placed in region II, it extends well into region III. Similarly, when the leading edge of the airfoil is placed in region I, it extends well into region II.

Figure 7 shows the pressure distributions with the inverted airfoil placed in regions I ($x/\ell = 0.10$), II ($x/\ell = 0.35$), and III ($x/\ell = 0.60$). It can be seen that the minimum pressure occurs at

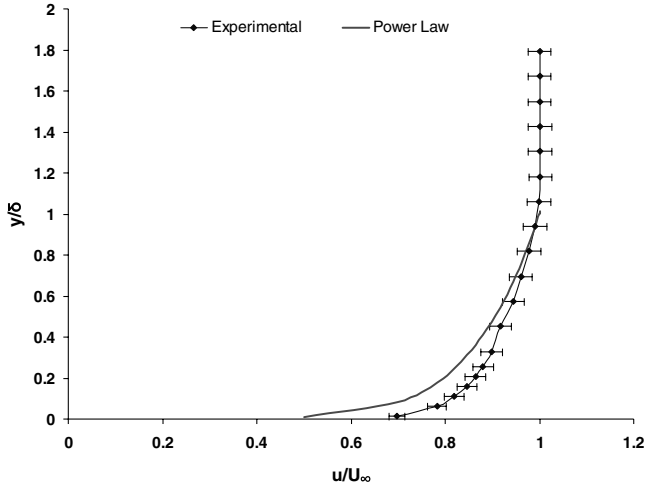

Fig. 10 Comparison of measured turbulent velocity profile with one-seventh power-law for the clean case.

the location of the separation bubble. The minimum value of C_p at this location is recorded to be around -0.725 for the clean case. This is followed by a strong pressure recovery. The pressure recovers back to a value of approximately $C_p = -0.15$. The accuracy of the measurement technique is clearly evident in Fig. 7. One would expect a straight line after the pressure recovery takes place [18]. Some fluctuations are observed between $x/\ell = 0.15$ and 0.45, which is because the liquid manometer rake did not contain enough manometers to obtain pressures from all 65 tappings at once. It is also important to note that because Fig. 7 shows the complete length of the flat plate, a slightly misleading view of the pressure under the separation bubble is observed. Quite a sharp decrease in C_p is seen at the onset of the separation bubble; however, this is not the case. The pressure does not increase sharply under the separation bubble, but instead remains almost constant. This was also observed by Crompton and Barrett [18]. However, a mild reduction in C_p under the separation bubble may be associated with the instrument uncertainty and other experimental errors. The maximum length of the separation bubble is estimated to be around 18.5 mm and it extends up to $x/\ell = 0.0285$ ($x = 28.5$ mm), as previously shown in the oil-flow picture in Fig. 4.

The graphs in Fig. 7 also clearly show that the inverted airfoil produces the effects of favorable pressure gradients on the flat plate (i.e., the pressure reduces in the freestream direction). When the inverted airfoil is placed in region I (near the leading edge of the flat plate), the upstream surface pressures are significantly reduced. A reduced value of C_p at the location of the separation bubble is evident in Fig. 7. This is because of the increase in freestream velocity that was observed in Fig. 5. Downstream of the inverted airfoil, a

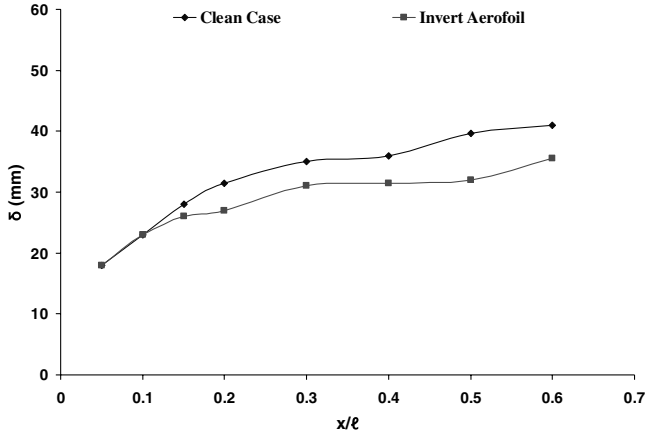

Fig. 11 Effects of the inverted airfoil on the δ profile.

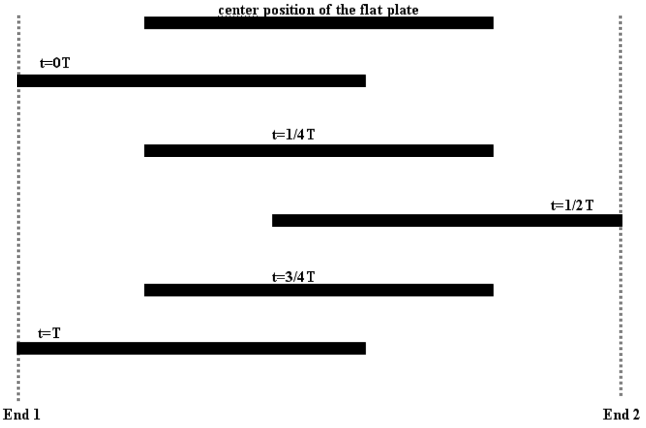

Fig. 13 Flat plate undergoing one complete oscillation cycle.

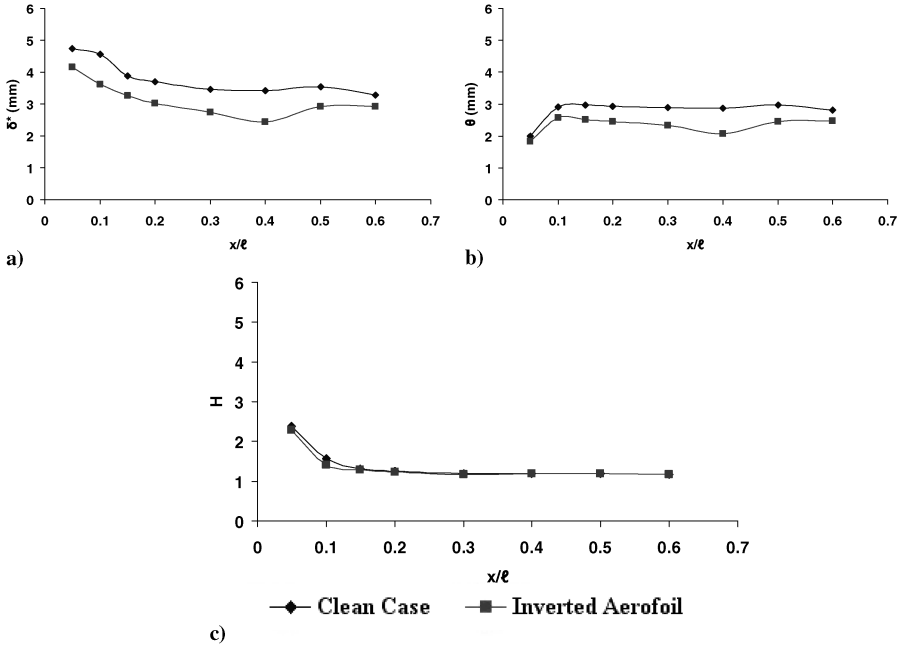

Fig. 12 Effects of the inverted airfoil on δ^*, θ, and H profiles.

reduction in surface pressures is observed over the entire length of the flat plate. When the inverted airfoil is placed in region II, a slight reduction in pressure is observed close to the leading edge. This is because the leading edge of the airfoil is placed well behind the leading edge of the flat plate in this case. The pressures then remain more or less the same until $x/\ell = 0.15$. Downstream of this location, a reduction in surface pressures is observed until $x/\ell = 0.85$. The effects of the pressure gradient observed with the inverted airfoil placed at $x/\ell = 0.35$ are higher than those observed at $x/\ell = 0.10$, mainly in regions II and III. When the inverted airfoil is placed in region III, the surface pressure is unaffected close to the leading edge. A reduction in surface pressures is not seen until $x/\ell = 0.35$. Downstream of this location, surface pressure reduces, but the effect is not as strong as when the airfoil is placed in either region I or II. The results therefore show that by placing the inverted airfoil in region II, desired pressure gradients effects are achieved, mainly in regions II and III. Figure 7 also shows that a steady value of the pressure toward the trailing edge of the flat plate with the inverted airfoil is lower than that with the clean case. But it expected that the pressures for each case would recover back to the clean-case value if the plate was longer and measurements were taken further downstream. The objective was to find the position of the inverted airfoil at which the imposed pressure gradients (favorable in this case) were the highest, and this is observed when the inverted airfoil was placed in Region II at $x/\ell = 0.35$. Hence, region II was chosen to place the inverted airfoil for all of the following experiments.

2. *Boundary-Layer Measurements*

For all of the velocity and turbulence intensity profiles plotted in this article, the first point of measurement starts $y = 0.5$ mm away from the surface. Figures 8 and 9 show the effects of the inverted airfoil on the mean velocity and turbulence intensity profiles (U_{rms}/U_∞). By placing the inverted airfoil in region II, the near-wall momentum increases at $x/\ell = 0.10$ (Fig. 8). By observing the velocity profiles at this location, it can be said that the reattachment of

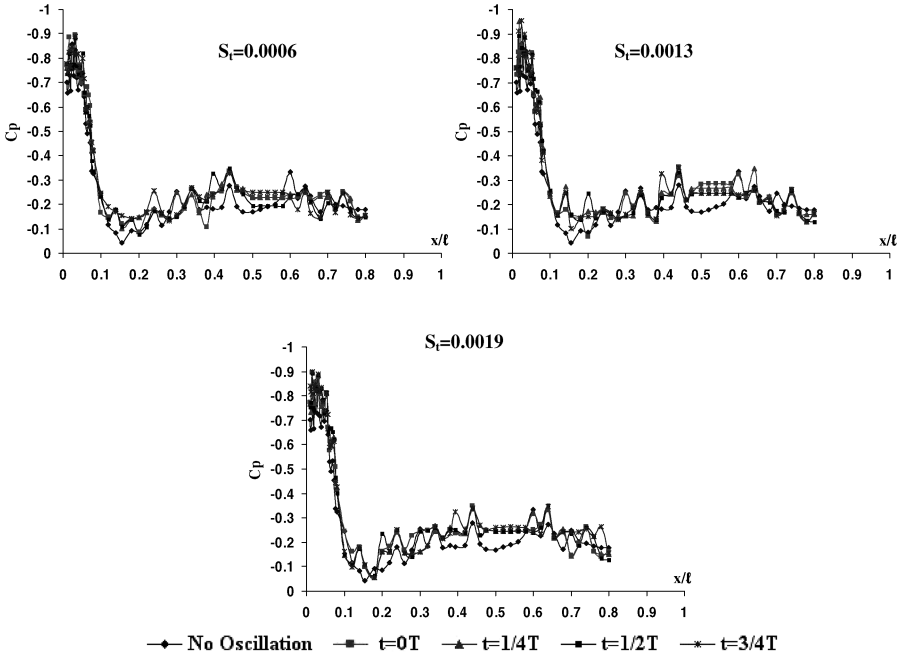

Fig. 14 Effects of oscillation at $A = 0.005$ m on instantaneous surface pressure.

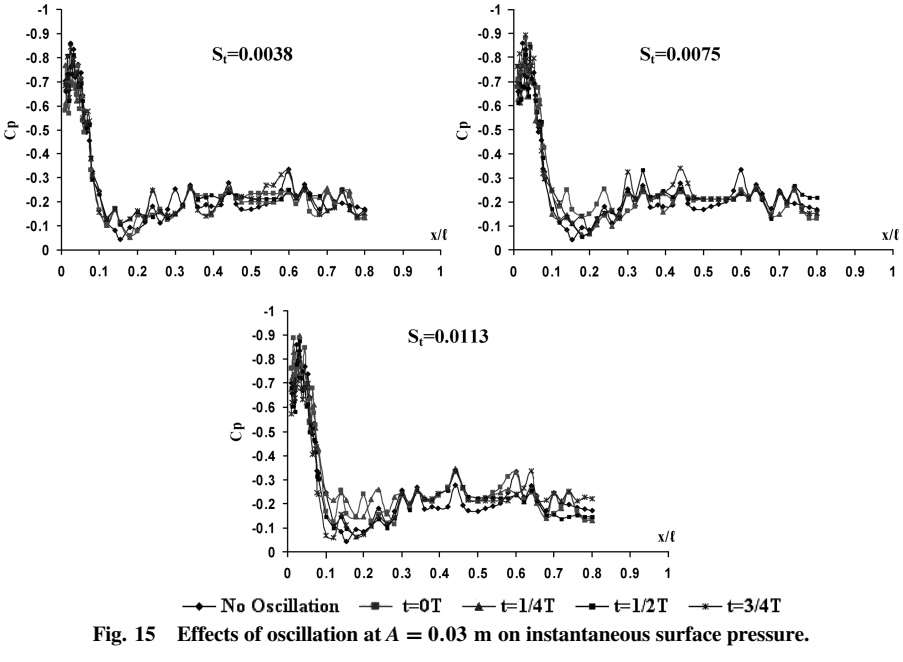

Fig. 15 Effects of oscillation at $A = 0.03$ m on instantaneous surface pressure.

the flow takes place earlier than that for the clean case. In both regions II and III, the velocity profiles remain unaffected. The turbulence intensity profiles in Fig. 9 show no changes in the turbulence levels in the downstream region of the flow. Regions II and III seem to be unaffected. However, reduced levels of turbulence are observed at $x/\ell = 0.10$. The presence of the inverted airfoil causes the turbulence intensity to reduce significantly near the wall region. At $x/\ell = 0.05$, where transition takes place just behind the leading-edge separation bubble, the turbulence intensity increases at near-wall region due to the inverted airfoil. It is believed that the inverted airfoil speeds up the reattachment process. The flow therefore becomes turbulent earlier than that for the clean case, and due to this, a reduction in turbulence intensities is observed at both $x/\ell = 0.05$ and 0.10.

Both Figs. 8 and 9 clearly show that the effects obtained by placing the inverted airfoil are small and it is hard to determine whether these differences are due to the experimental errors or not. A comparison was therefore made between the turbulent velocity plotted in Fig. 8 and that obtained using the power-law equation given next:

$$\frac{u}{U_\infty} = \left(\frac{y}{\delta}\right)^{1/7} \tag{2}$$

Figure 10 provides a comparison of the measured steady turbulent boundary-layer velocity profile (at $x/\ell = 0.60$) with the one-seventh power-law velocity profiles, which is well known in the literature [19]. It can be seen that theory predicts a lower velocity near the wall region of the flat plate. However, the shape of both the measured velocity profile and that obtained using the one-seventh power law is similar. One possible reason behind the difference could be the thickness of the boundary layer in this case. As we will examine later, due to the existence of the leading-edge separation bubble, the boundary-layer thickness on the flat plate increases abruptly. Also shown in Fig. 10 are the error bars on the experimental velocity profile. Clearly, the uncertainties are large, and therefore any small differences observed due to the inverted airfoil (Figs. 8 and 9) could actually be due to the experimental errors. However, where significant differences are seen, such as in the transitional region of the flow, it can be concluded that these changes are due to favorable pressure gradients imposed by the inverted airfoil.

The effects of the inverted airfoil were examined on the boundary-layer thickness δ at each location. Figure 11 shows that the boundary layer becomes thinner with the inverted airfoil placed in region II. In the transitional region (i.e., at $x/\ell = 0.05$), δ is unaffected. The maximum effect is seen in regions II and III. The results therefore show that the inverted airfoil produces favorable pressure gradients on the flat plate.

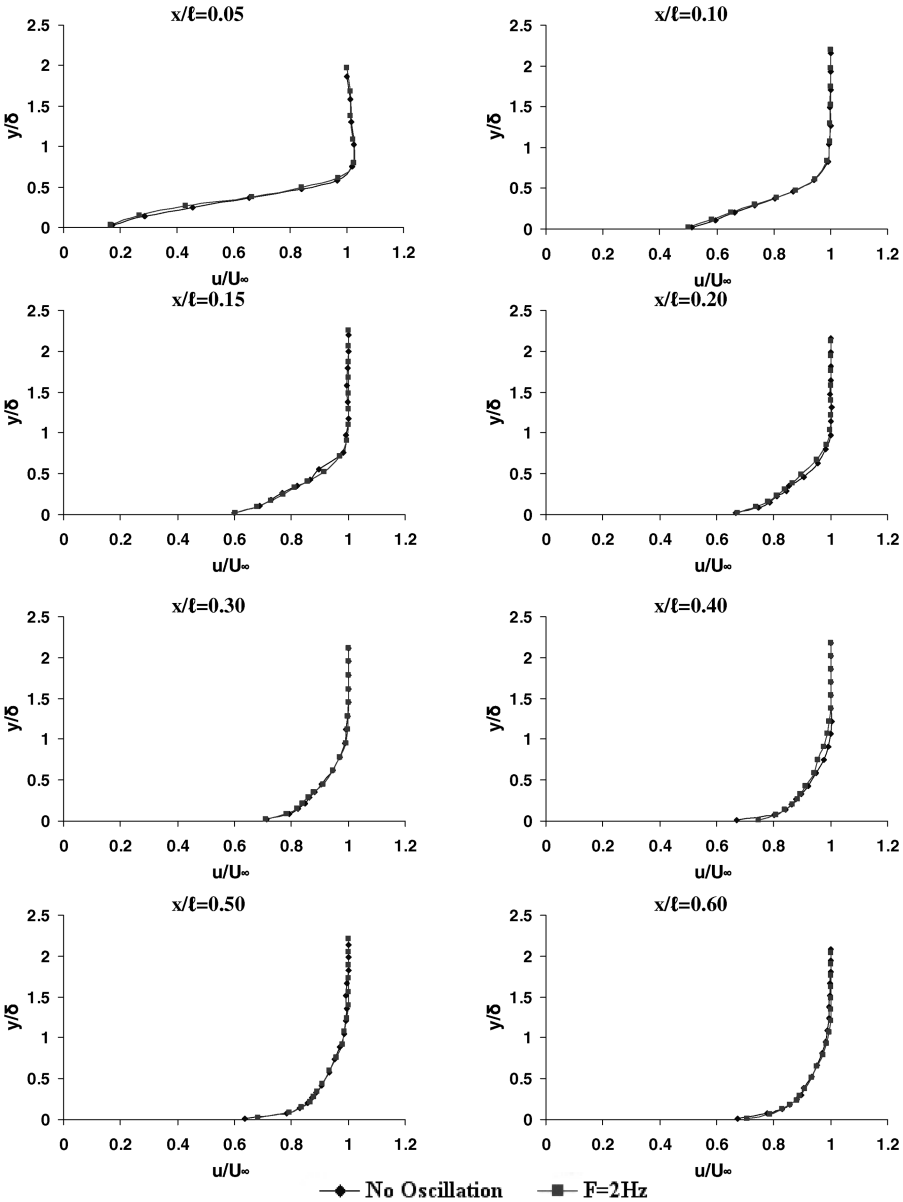

Fig. 16 Effects of oscillation at $S_t = 0.0006$ on time-averaged velocity profiles.

To make a more quantitative assessment, we will now examine the distributions of boundary-layer integral parameters: namely, the boundary-layer displacement thickness δ^*, momentum thickness θ, and shape factor H. The parameters are defined as given next:

$$\delta^* = \int_0^{\delta} \left(1 - \frac{u}{U_\infty}\right) \mathrm{d}y \tag{3}$$

where u is the local velocity, U_∞ is the velocity at the edge of the boundary layer, and y is the displacement from the surface. The momentum thickness is given by

$$\theta = \int_0^{\delta} \frac{u}{U_\infty}\left(1 - \frac{u}{U_\infty}\right) \mathrm{d}y \tag{4}$$

The displacement thickness is an indicator of how much the external inviscid flow is deflected by the viscous boundary layer, with adverse pressure gradients and separation causing an increase in δ^*. Further, separation is known to occur [20,21] when $2 < H < 2.8$, so that we can assess how far the flow is removed from the incipient separation condition. The shape factor H is therefore given by

$$H = \frac{\delta^*}{\theta} \tag{5}$$

Figure 12 shows the effect of favorable pressure gradients on the boundary-layer displacement thickness δ^*, momentum thickness θ, and shape factor H. Even though δ is unaffected in the transitional region, Fig. 12 shows that the displacement thickness δ^* reduces significantly throughout the entire flat plate. A reduction in momentum thickness θ is also seen in all three regions of the flow (Fig. 12). The shape factor, however, remains mostly unaffected in both regions II and III. However, a slight reduction in the value of H in region I suggest that the pressure gradients speed up the reattachment process, as previously observed in Fig. 8.

B. Case B: With Oscillation

Figure 13 shows a graphical representation of the movement of the flat-plate model when it undergoes one complete oscillation cycle. One complete oscillation cycle of the flat plate is divided into 4 phases: $t = 0T$ represents the beginning of the measurements, $t = \frac{1}{4}T$ represents the point at which the plate has completed one-fourth of its oscillation cycle, $t = \frac{3}{4}T$ represents the point at which the plate

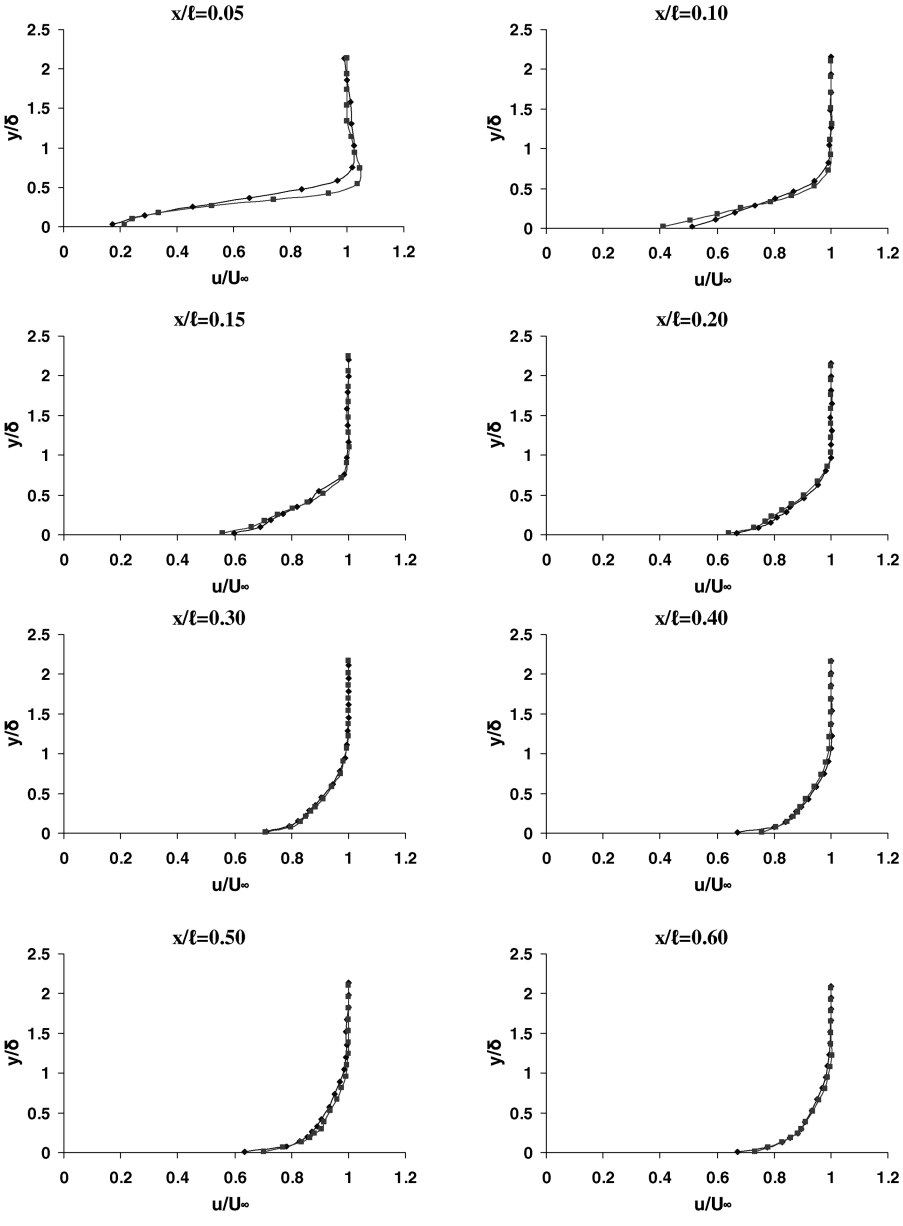

Fig. 17 Effects of oscillation at $S_t = 0.0038$ on time-averaged velocity profiles.

has completed three-fourths of its oscillation cycle, and $t = T$ represents the point at which the flat plate has completed one oscillation cycle. The pressure at $t =$ T would be the same as that at $t = 0T$. The plate was allowed to oscillate for 4 s in all cases and the data were captured. The pressure at any given point within an oscillation cycle was deduced from the data recorded. A triggering mechanism was designed and placed in the wind tunnel to ensure consistency in the data and a known and common starting point for all measurements in the oscillation cycle.

Figure 14 shows the effects of oscillation at an amplitude equal to 0.005 m on instantaneous surface pressure. Increased levels of pressure can be seen in region II [which extends from $x/\ell = 0.2$ to 0.4 (Fig. 2)] of the flow. This effect gets stronger with increasing Strouhal number S_t. The pressure remains mainly unaffected near the leading edge of the flat plate (i.e., in the region in which the separation bubble exists). The increased pressures are observed during all 4 phases of oscillation. In region III, the pressure remains unchanged by oscillation. The results therefore show that under the influence of favorable pressure gradients, oscillation affects pressure in the region in which the flow is still at the late stages of its transition to turbulence.

When the amplitude is increased to 0.03 m (Fig. 15), the effects due to oscillation are only seen at $S_t = 0.0113$. In region II, just downstream of $x/\ell = 0.10$, an increase in pressure is observed at $t = 0$ T. At this phase, the flat plate is moving in the direction of the freestream. Slight changes in pressures are also seen in region II, but the effects are not as strong as previously seen in Fig. 14. The results therefore suggest that the amplitude of oscillation has a major influence on surface pressures. The favorable effects increase with increasing S_t at both amplitudes of oscillation.

It is conjectured that the wall oscillation at higher frequencies may trigger new disturbances in the flowfield that might effect the growth of the boundary layer. As a result, as the Strouhal number increases, the favorable effects due to the inverted airfoil become stronger. However, it is difficult to draw any conclusions from the pressure measurements alone.

It is important to note that both the velocity and turbulence intensity profiles presented in the following sections were time-averaged. The oscillation system was not phase-locked as was done for the pressure-measurement case. The flat plate was therefore allowed to oscillate for 4 s in all cases, and the data were captured at a sampling rate of 2 kHz.

Figures 16 and 17 show the effect of oscillation on time-averaged velocity profiles at amplitudes of 0.005 and 0.03 m, respectively. Velocity profiles at $S_t = 0.0006$ (Fig. 16) show no change due to oscillation. However, a slight increase in the flow momentum near

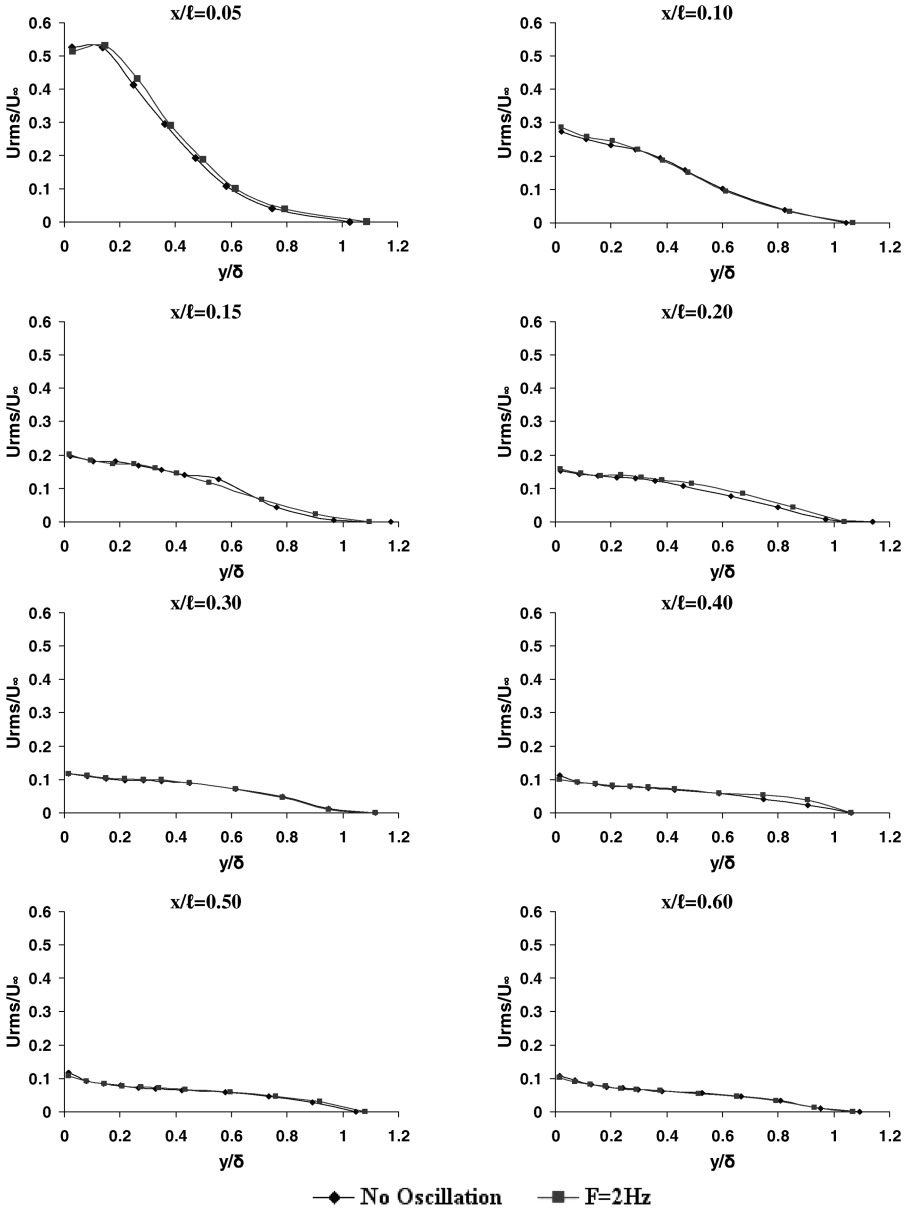

Fig. 18 Effects of oscillation at $S_t = 0.0006$ on time-averaged turbulence intensity profiles.

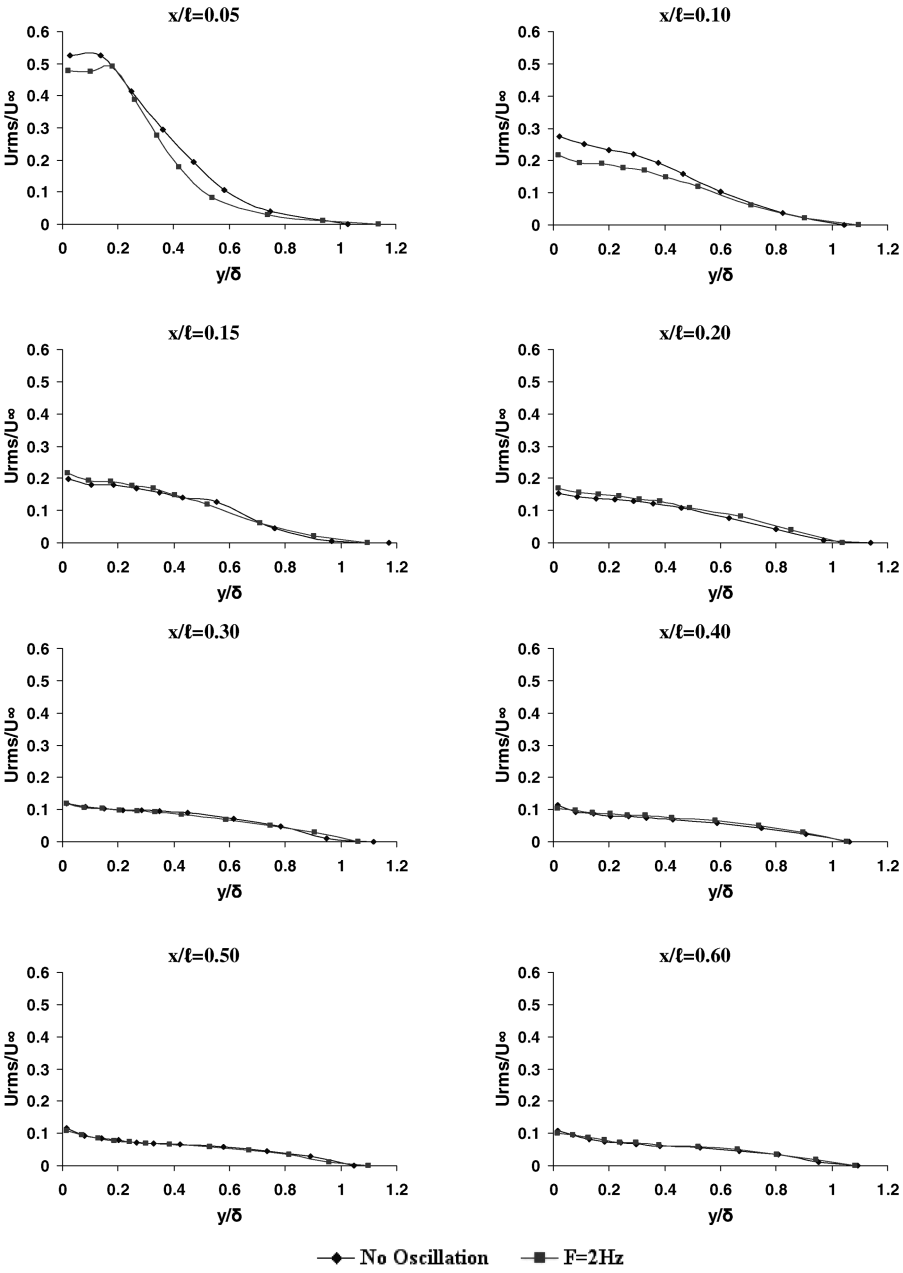

Fig. 19 Effects of oscillation at $S_t = 0.0038$ on time-averaged turbulence intensity profiles.

the wall region is observed in region III (i.e., between $x/\ell = 0.40$ and 0.60) of the flow. At $x/\ell = 0.40$, the flow velocity near the surface of the flat plate increases. This effect gets smaller in the downstream direction at $x/\ell = 0.50$ and 0.60. Regions I and II remain mainly unaffected at lower amplitudes of oscillation. At an amplitude equal to 0.005 m, velocity profiles at $S_t = 0.0013$ and 0.0019 showed similar changes due to oscillation.

When the amplitude of oscillation is increased to 0.03 m ($S_t = 0.0038$) (Fig. 17), changes in velocity profiles are seen in region I. At $x/\ell = 0.05$, the flow gains momentum near the wall region and continues to accelerate within the boundary layer. However, at $x/\ell = 0.10$, the flow is decelerated at the near-wall region due to oscillation. It then reaccelerates at $y/\delta = 0.18$. The flow velocity continues to increase in magnitude until it reaches the freestream value. The velocity profile at $x/\ell = 0.10$ also shows that oscillation slows the reattachment process, making the profile less full. Both regions II and III are unaffected by oscillation, because the velocity profiles remain the same as that for the no-oscillation case. At an amplitude equal to 0.03 m, velocity profiles at $S_t = 0.0075$ and 0.0113 showed similar changes due to oscillation.

Figures 18 and 19 show the effect of oscillation on the turbulence intensity profiles at amplitudes of 0.005 and 0.03 m, respectively. The turbulence levels in Fig. 18 remain unaffected at $S_t = 0.0006$. The results correlate with the velocity profiles seen in Fig. 16. Even though the flow near the wall region gained momentum in region III, the turbulence intensities remain unaffected. When the amplitude of oscillation is increased to 0.03 m ($S_t = 0.0038$) (Fig. 19), changes in turbulence levels are seen in region I. At $x/\ell = 0.05$, the turbulence

Table 1 Summary of cases tested with oscillation

A, m	F, Hz	S_t
0.005	2	0.0006
	4	0.0013
	6	0.0019
0.03	2	0.0038
	4	0.0075
	6	0.0113

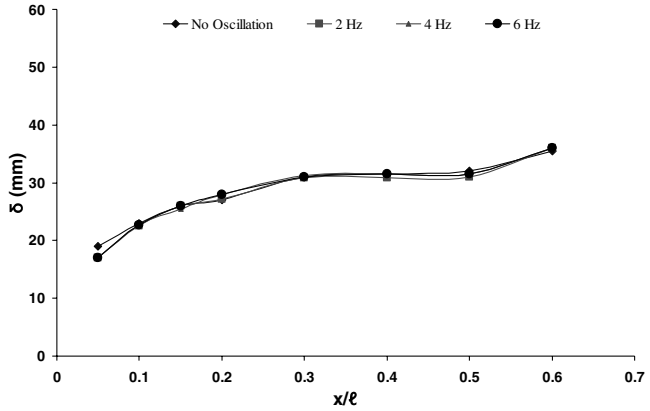

Fig. 20 Effects of oscillation at $A = 0.005$ m on boundary-layer thickness.

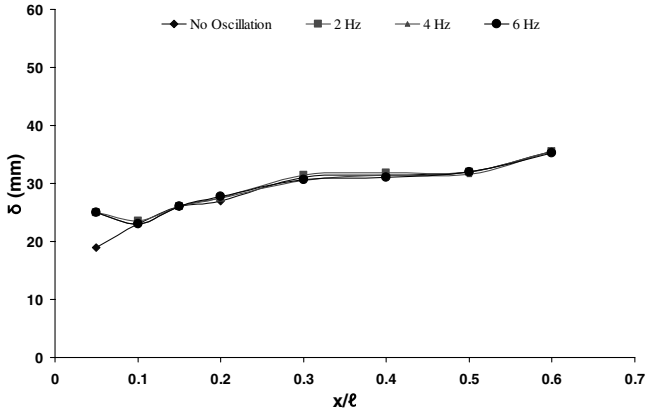

Fig. 21 Effects of oscillation at $A = 0.03$ m on boundary-layer thickness.

level near the wall region reduces and continues to be lower within the boundary layer. At $x/\ell = 0.10$, turbulence levels are significantly reduced near the wall region. This effect diminishes at $y/\delta = 0.6$. It is believed that the inverted airfoil sheds periodic vortices into the flow that alter the turbulence levels. During the oscillation, this effect is further enhanced; however, the disturbances created by the shedding frequency do not penetrate well into the outer layer of the boundary layer. Because of this reason, the effects of oscillation are only seen slightly higher than at half of the boundary-layer depth at $x/\ell = 0.10$. Upstream of this location, the turbulence intensity is unaffected by oscillation. Regions II and III remain largely unaffected by oscillation. The turbulence intensities remain the same downstream of $x/\ell = 0.10$.

The results for the oscillation case presented in the current paper show two of the six test cases mentioned in Table 1. With the amplitude of oscillation kept at 0.005 m, the effect of increasing frequency was also examined on both the time-averaged velocity and turbulence intensity profiles. The results showed similar trends to those seen in Figs. 16 and 18. It was found that by increasing the frequency and keeping the amplitude constant, no significant effects were observed. Similar observations were also made for higher-amplitude cases. The results clearly show that the slight changes observed due to the changes in Strouhal number at constant amplitude relate to the instrument uncertainty itself. The hot-wire uncertainty in the velocity measurements was estimated to be $\pm 2.5\%$. Therefore, it can be concluded that the changes observed are due to measurement errors.

Boundary-layer thickness δ was determined at each location at an amplitude of oscillation equal to 0.005 m. Figure 20 shows no changes in δ due to oscillation. The effect of increasing S_t also has no affect on δ at lower amplitudes of oscillation. However, when the amplitude is increased to 0.03 m (Fig. 21), δ increases significantly in region I. An increment in δ in this region correlates to the mean velocity and turbulence intensity profiles in Figs. 18 and 19, respectively. The results therefore show that the effects of oscillation are observed only at higher amplitudes of oscillation and that region I (which is transitional in nature) is mainly affected.

The effects of oscillation at an amplitude of 0.005 m on δ^*, θ, and the shape factor H are shown in Fig. 22. Both δ^* and θ remain mostly unchanged in all of the regions of the flow. However, only slight changes are observed at different locations along the flat plate. These changes are well within the measurement uncertainties. The shape-factor profile also remains the same, as seen in Fig. 22c.

When the amplitude of oscillation is increased to 0.03 m, δ^* and θ remain unaffected in regions II and III. However, at $x/\ell = 0.05$ in region I, as expected, there is only a slight increases in both δ^* and θ. This is because the boundary-layer thickness increases at this location, as seen in Fig. 21. The shape-factor profile in Fig. 23c remains unaffected throughout the flat plate, even though the velocity profiles at $x/\ell = 0.05$ and 0.10 in Fig. 17 showed that oscillation tends to slow the reattachment process. However, the value of H in Fig. 23c shows no changes at all. One possible reason could be because of the inaccuracies of hot-wire measurements. This might have affected the calculation of integral parameters such as the displacement thickness and the momentum thickness. As a result, the values of the shape factor might have inaccuracies as well.

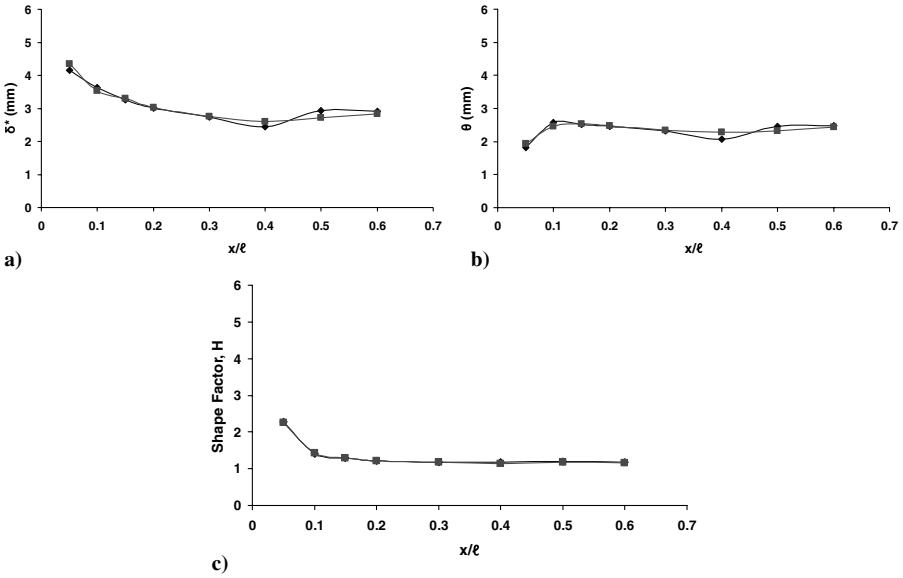

Fig. 22 Effects of oscillation at $S_t = 0.0006$ on δ^*, θ, and H profiles.

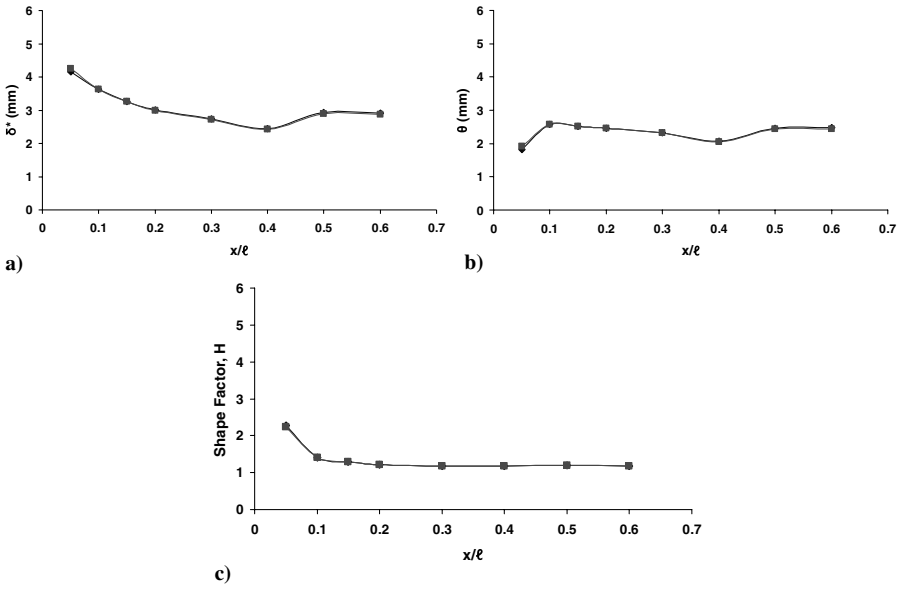

Fig. 23 Effects of oscillation at $S_t = 0.0038$ on δ^*, θ, and H profiles.

The results clearly show that when the flat plate is under the influence of favorable pressure gradients, the time-averaged velocity and turbulence intensity profiles remain unaffected in both regions II and III, in which the flow is turbulent (see Fig. 2). At higher amplitudes of oscillation, the boundary-layer thickness increases just downstream of the separation bubble at $x/\ell = 0.05$ in region I. At this location, slight changes in other boundary-layer properties (boundary-layer displacement thickness and momentum thickness) are also observed. However, the overall shape factor remains unchanged at both amplitudes of oscillation. It is conjectured that oscillation changes the size and location of the separation bubble, and due to this reason, most changes in the boundary-layer properties are observed in this region of the flow.

However, under the influence of adverse pressure gradients [17] when the cylinder is placed in region II, the effect of the wake interaction with the flat-plate boundary layer speeds up the reattachment process in region I. As a result, the velocity profiles in this region are modified and the shape-factor value reduces as well. The flow in the leading-edge region just downstream of the separation bubble exhibits an oscillatory behavior, with the number of cycles increasing with increasing Strouhal number. This may be associated with the presence of the separation bubble and the influence that the flat-plate oscillation may have on its structure, properties, and characteristics. Because of this reason, the boundary-layer thickness also increases at higher amplitudes of oscillation in the transitional region in the present case and also in our previous studies [17].

V. Conclusions

The flow separates very near the rounded leading edge, causing the formation of a separation bubble. The presence of the separation bubble forces transition, causing the thickening of the boundary layer. The freestream velocity inside the wind-tunnel test section changes in the presence of the inverted airfoil. Increased freestream velocities both upstream and downstream of its location are observed. The inverted airfoil increases surface pressures along the flat plate. For the region I case, its effect is seen along the entire length of the flat plate. The effect of the inverted airfoil is more pronounced in the region II case. For the region III case, its effect is only seen downstream of $x/\ell = 0.35$. Both mean velocity and turbulence intensity profiles are affected at various locations along the flat plate. The shape factor remains mostly unchanged in all of the regions, although significant reductions in both displacement and momentum thickness are observed in regions throughout the flat plate.

Oscillation causes increased levels of pressure in region II of the flow. With increasing Strouhal number, the effects get stronger at both low and high amplitudes of oscillation. Both mean velocity and turbulence intensity profiles remain unaffected at low amplitudes of oscillation. When the amplitude is increased to $A = 0.03$ m, changes in mean velocity and turbulence intensity profiles are observed in region I only. Boundary-layer thickness therefore increases at $x/\ell = 0.05$ due to oscillation at $A = 0.03$ m. The boundary-layer properties (such as the boundary-layer displacement thickness, momentum thickness, and the shape factor) all remain more or less the same. However, in region I, in which the flow is in its transitional state, oscillation slows the reattachment process under the influence of favorable pressure gradients.

More precise measurement techniques need to be employed to study the complete structure of the flow in the boundary layer, because this is not possible from the hot-wire measurements alone. Hot-wire anemometry is not adequate to measure reversed flow such as the flow in the vicinity of the separation bubble; therefore, investigations are now being performed using computational fluid dynamics, and experiments are also being performed using a particle image velocimetry system. The results from these experiments will help us understand the physical mechanisms associated with streamwise oscillations under the influence of favorable pressure gradients.

Acknowledgments

The authors would like to thank the Overseas Research Scheme (ORS) for their financial support and Neel Shah for his assistance in the investigation.

References

[1] Favre, A., "Contribution a L'etude Experimentale Des Mouvements Hydrodynamques a Deux Dimensions," Ph.D. Thesis, Univ. of Paris, Paris, 1938.

[2] Modi, V. J., Fernando, M. S. U. K., and Yokomiz, T., "Moving Surface Boundary-Layer Control: Studies with Bluff Bodies and Application," *AIAA Journal*, Vol. 29, No. 9, Sept. 1991, pp. 1400–1406. doi:10.2514/3.10753

[3] Modi, V. J., "Moving Surface Boundary Layer Control: A Review," *Journal of Fluids and Structures*, Vol. 11, No. 6, Aug. 1997, pp. 627–663. doi:10.1006/jfls.1997.0098

[4] Rott, N., "Unsteady Viscous Flow in the Vicinity of Stagnation Point," *Quarterly of Applied Mathematics*, Vol. 13, No. 3, 1956, pp. 444–451.

[5] Sears, W. R., "Some Recent Developments in Airfoil Theory," *Journal of the Aeronautical Sciences*, Vol. 23, No. 11, 1956, pp. 490–499.

[6] Moore, F. K., "On the Separation of the Unsteady Laminar Boundary Layer," *Boundary Layer Research*, edited by H. Gortler, Springer–Verlag, Berlin, 1958, pp. 296–310.
[7] Bott, D. M., and Bradshaw, P., "Effect of High Freestream Turbulence on Boundary-Layer Skin Friction and Heat Transfer," Mechanical Engineering Dept., Stanford Univ., Rept. MD-75, Stanford, CA, 1997.
[8] Uzkan, T., and Reynolds, W. C., "A Shear-Free Turbulent Boundary Layer," *Journal of Fluid Mechanics*, Vol. 28, July 1967, pp. 803–821. doi:10.1017/S0022112067002459
[9] Thomas, N. H., and Hancock, P. E., "Grid Turbulence Near a Moving Wall," *Journal of Fluid Mechanics*, Vol. 82, Sept. 1977, pp. 481–496. doi:10.1017/S0022112077000792
[10] Aronson, D., Johannson, A. V., and Lofdahl, L., "Shear Free Turbulence Near a Wall," *Journal of Fluid Mechanics*, Vol. 338, May 1997, pp. 363–385. doi:10.1017/S0022112097005065
[11] Hunt, J. C. R., and Graham, J. M. R., "Free Stream Turbulence Near Plane Boundaries," *Journal of Fluid Mechanics*, Vol. 84, Jan. 1978, pp. 209–235. doi:10.1017/S0022112078000130
[12] Perot, J. B., and Moin, P., "Shear Free Turbulent Boundary Layers," *Journal of Fluid Mechanics*, Vol. 295, July 1995, pp. 199–227. doi:10.1017/S0022112095001935
[13] Karniadakis, G. E., and Choi, K. S., "Mechanisms on Transverse Motions in Turbulent Wall Flows," *Annual Review of Fluid Mechanics*, Vol. 35, 2003, pp. 45–62. doi:10.1146/annurev.fluid.35.101101.161213
[14] Du, Y., Symeonidis, V., and Karniadakis, G. E., "Drag Reduction in Wall Bounded Turbulence via a Transverse Travelling Wave," *Journal of Fluid Mechanics*, Vol. 457, Apr. 2002, pp. 1–34.
[15] Choi, K. S., DeBisschop, J. R., and Clayton, B. R., "Turbulent Boundary Layer Control by Means of Spanwise-Wall Oscillation," *AIAA Journal*, Vol. 36, No. 7, 1998, pp. 1157–1163. doi:10.2514/2.526
[16] Choi, K. S., and Clayton, B. R., "The Mechanism of Turbulent Drag Reduction with Wall Oscillation," *International Journal of Heat and Fluid Flow*, Vol. 22, No. 1, Feb. 2001, pp. 1–9. doi:10.1016/S0142-727X(00)00070-9
[17] Amir, M., and Kontis, K., "Effect of Oscillation on Boundary-Layer Development Under the Influence of Adverse Pressure Gradients," *Journal of Aircraft*, Vol. 44. No. 3, May 2007, pp. 875–887. doi:10.2514/1.25450
[18] Crompton, M. J., and Barrett, R. V., "Investigation of the Separation Bubble Formed Behind the Sharp Leading Edge of a Flat Plate at Incidence," *Proceedings of the Institution of Mechanical Engineers, Part G (Journal of Aerospace Engineering)*, Vol. 214, No. 3, 2000, pp. 157–176. doi:10.1243/0954410001531980
[19] Schlichting, H. T., *Boundary Layer Theory*, McGraw–Hill Series in Mechanical Engineering, McGraw–Hill, New York, 1979.
[20] Young, A. D., *Boundary Layers*, Blackwell Science, Boston, 1989.
[21] Schlichting, H., and Gersten, H., *Boundary Layer Theory*, 8th ed., Springer, New York, 2000.